Eulerian models and algorithms for unbalanced optimal transport

Damiano Lombardi, Emmanuel Maitre

Eulerian models and algorithms for unbalanced optimal transport

Damiano Lombardi

Equipe REO, INRIA Rocquencourt.
e-mail: damiano.lombardi@inria.fr

Emmanuel Maitre

Laboratoire Jean Kuntzmann,
Grenoble University and CNRS.
e-mail: emmanuel.maitre@imag.fr

Abstract: Benamou and Brenier formulation of Monge transportation problem [4] has proven to be of great interest in image processing to compute warpings and distances between pair of images [2]. One requirement for the algorithm to work is to interpolate densities of same mass. In most applications to image interpolation, this is a serious limitation. Existing approaches [3, 15, 16] to overcome this caveat are reviewed, and discussed. Due to the mix between transport and L^2 interpolation, these models can produce instantaneous motion at finite range. In this paper we propose new methods, parameter-free, for interpolating unbalanced densities. One of our motivations is the application to interpolation of growing tumor images.

AMS 2000 subject classifications: Primary 60K35, 60K35; secondary 60K35.

1. Introduction

1.1. Context in image processing

Optimal transportation has found a wide field of application in image interpolation and registration, since pioneering works of Benamou and Brenier [4] who introduced an algorithm based on the minimization of the kinetic energy by flows which preserves the mass. By structure, optimal transportation requires initial and final densities to be balanced, that is, of equal mass.

In real applications, this is seldom the case, either because images are projections of a 3D reality, or picture a growing object (e.g. tumor), or simply due to noise. Benamou [3] proposed a way to tackle this latter problem. His approach was to find a compromise between an L^2 projection and an optimal transport. He considered the optimal transportation between the initial density and a final density of same mass, which was computed by minimizing its L^2 distance with the real final density. This produces a transport between the larger (in the L^2 meaning) part of the densities. Note that a weight is present in the method (see below) in front of this L^2 distance, and it is acknowledged in [3] that this parameter choice could be problematic in some cases.

At a late stage of redaction of this article, we got aware of the work of Piccoli and Rossi [15, 16], who studied theoretically optimal transportation with source terms, generalizing Benamou's approach. In particular, they obtained an interpolated distance between the L^2 and Wasserstein metrics, and exhibit interesting properties of this new distance. Another approach to unbalanced optimal transport was proposed by Figalli and Gigli in [11] (see also [1]). Their approach is to consider the boundary as a source/sink of mass.

Our main concern is to provide a notion of generalized optimal transport interpolation between measures/densities of different mass that could apply to the study of tumors growth. Therefore we do not want to involve the picture boundary as in [11], as far as mass is concerned. Rather, we will consider in our test cases isolated tumors (for real pictures) or isolated gaussians (for synthetic ones), between which growth occurs, but not by mass coming from the boundary. Likewise, we would like to avoid the "infinite speed" of L^2 interpolation that is inherent to the approach of [3] and [15, 16]. In these two approaches, indeed, due to the fact that the resulting generalized interpolation mixes Wasserstein and L^2 metrics, some mass at positive distance of the initial tumor support could instantaneously appear on the interpolating path, which is undesirable for a tumor growth model.

We will rather try to define possibly non linear source terms, since once again our application is oriented toward tumor growth images, that is, the mass variation is not to be neglected and has a real meaning. In the following, we introduce several models that transport unbalanced densities. Our aim is to address the optimal transportation problem between two densities (images) which represent an object which has grown between two instants. These models are based on a modification of the projection method hidden in Benamou-Brenier algorithm, where a source term is added. We first recall some basic facts about optimal transportation, then the solution proposed by Benamou. Next we present our algorithms, discuss some of their properties, and study how they behave on several tests cases.

1.2. Quick introduction to optimal transportation

Let Ω be an open bounded domain and let us consider the Monge problem of pushing one measure μ to another measure ν, through a transportation map which minimizes some cost. The standard setting assume that the measures μ and ν are absolutely continuous with respect to the Lebesgue measure, of densities ρ_0 and ρ_1, nonnegative on Ω, and of equal mass:

$$\int_\Omega \rho_0(x)dx = \int_\Omega \rho_1(x)dx = 1.$$

In application to image processing, these densities will correspond to gray levels, and in general this condition would not be satisfied. A map $T : \Omega \to \Omega$ is a transfer map from ρ_0 to ρ_1 if for every subset $A \subset \Omega$,

$$\int_A \rho_1(x)dx = \int_{\{T(x)\in A\}} \rho_0(x)dx. \tag{1}$$

If T is a $\mathcal{C}^1$ mapping, then by a change of variables this is equivalent to

$$\det(\nabla T(x))\rho_1(T(x)) = \rho_0(x),$$

which is under-determined. Let $\Gamma(\rho_0, \rho_1)$ be the set of mappings T transfering ρ_0 on ρ_1. The L^p Kantorovich-Wassertein distance between ρ_0 and ρ_1 is then defined by

$$d_p(\rho_0, \rho_1)^p = \inf_{T\in\Gamma(\rho_0,\rho_1)} \int |T(x) - x|^p \rho_0(x)dx.$$

The L^p Monge-Kantorovitch problem (MKP) corresponds to find a mapping T such that this infimum is achieved.

In the case $p = 2$, the problem admits an unique solution (see e.g. Villani [17] page 66), which is the gradient of a convex fonctional from Ω to $\mathbb{R}$:

$$T(x) = \nabla\Psi(x).$$

The convex function Ψ is solution of Monge-Ampère equation:

$$\det(D^2\Psi)\rho_1(\nabla\Psi(x)) = \rho_0(x).$$

This equation being highly nonlinear, numerical methods to solve the MKP problem based on discretization of the Monge-Ampère equation have already been investigated [13, 10, 7, 8]. In application to image morphing problem, it is relevant to seek a time-dependent family of mappings $T(\cdot, t)$ transfering continuously ρ_0 to ρ_1. In [4] the authors introduced a fluid mechanics formulation of MKP, by adding a new dimension to the original problem (the time). The idea is to consider an arbitrary time interval $[0, t_m]$ and all functions $\rho(x, t) \geq 0$ and vector fields $v(x, t) \in \mathbb{R}^n$ solution of the continuity conditions with prescribed initial and final densities:

$$\partial_t\rho + \operatorname{div}(\rho v) = 0, \qquad \rho(x, 0) = \rho_0(x), \quad \rho(x, t_m) = \rho_1(x), \tag{2}$$

and homogeneous Dirichlet conditions on $\partial\Omega$. Then we have :

Theorem 1 (Benamou-Brenier). *In the case $p = 2$ the KW distance between ρ_0 and ρ_1 is such that:*

$$d_2(\rho_0, \rho_1)^2 = \inf t_m \int_\Omega \int_0^{t_m} \rho(x,t)|v(x,t)|^2 dxdt$$

the infimum being taken on ρ, v verifying (2).

This approach is numerically solved using a saddle-point problem based on a augmented Lagrangian method. In the last few years, others applications of optimal transportation methods to image analysis have been proposed. For instance, instead of solving the saddle-point problem directly, Angenent et al. derived a novel gradient flow for the computation of the optimal transport map [2]. Unfortunately, all these methods require that the initial and final densities have the same mass. This can be seen directly on the mass conservation constraint (2) upon integration in time and space, using periodic or Dirichlet boundary conditions on v on $\partial\Omega$.

The remaining of this paper is organized as follows: in the next section, after having recalled some existing solution to this problem of unbalanced densities, we consider a new optimal transport dealing with the different mass of densities. Several source terms are considered and compared, and numerical tests are performed.

2. Some existing models of unbanlanced mass transportation

The starting point of this article is the Benamou-Brenier fluid mechanics formulation of the L^2-MKP [4]. Consider $\Omega = (0,1)^2$ with Dirichlet boundary conditions and a time interval $[0, t_m]$, we set $Q_m = \Omega \times (0, t_m)$. In order to minimize the energy under the constraint (2), we first introduce the new variables ρ and $m = \rho v$ (into which the constraint expresses linearly) and we consider the (convex) problem:

$$\inf_{(\rho,m)\in C(\rho_0,\rho_1)} t_m \int_\Omega \int_0^{t_m} \frac{|m|^2}{2\rho} dxdt$$

where

$$C(\rho_0,\rho_1) = \{(\rho, v),\ \partial_t\rho + \operatorname{div} m = 0,\ \rho(\cdot,0) = \rho_0,\ \rho(\cdot,t_m) = \rho_1 \text{ on } \Omega,\ m\cdot n = 0 \text{ on } \partial\Omega\times(0,t_m)\}\,. \quad (3)$$

Note that upon space integration of the conservation equation in (3), we still get

$$\int_\Omega \rho_0(x)dx = \int_\Omega \rho_1(x)dx. \quad (4)$$

In order to deal with unbalanced densities, Benamou proposed to somehow mix the L^2 and Wasserstein distances. Given a parameter $\gamma > 0$, one minimizes

$$d_W(\rho_0, \tilde\rho_1)^2 + \gamma\|\tilde\rho_1 - \rho_1\|_{L^2}^2$$

among all densities $\tilde\rho_1$ of same mass as ρ_0. While tests performed by Benamou showed that this algorithm allows to correctly compute interpolation between two densities with underlying noise, we observe that it is easy to find examples where, for γ large enough, $\tilde\rho_1$ could be negative. This is the case for instance if ρ_0 is a gaussian of weight 1, while ρ_1 is the sum of two gaussians functions of weights 1 and 2 (we insist that this kind of examples was not under the scope of the method developed in [3]). Then taking large γ would lead to lower significantly ρ_1 so that its smaller part could become negative. This is highly undesirable in the context we are considering.

A very related model of optimal transport with source term has been recently introduced by Piccoli and Rossi in two papers [15, 16]. In the first work, they provide a link between a transport equation with source term and a generalized Wasserstein distance, whereas the second paper introduces and studies the Benamou-Brenier formula in the case of unbalanced mass densities. More precisely, they proved that the generalized Wasserstein distance defined by

$$W_2^{a,b}(\rho_0,\rho_1)^2 = \inf_{\tilde\rho_0,\tilde\rho_1\in L^1_+(\Omega), \|\tilde\rho_0\|_1 = \|\tilde\rho_1\|_1} a^2(\|\tilde\rho_0 - \rho_0\|_1 + \|\tilde\rho_1 - \rho_1\|_1)^2 + b^2 W_2(\tilde\rho_0,\tilde\rho_1)^2$$

coincides with the generalized Benamou-Brenier formula, ie one has also:

$$W_2^{a,b}(\rho_0,\rho_1)^2 = \inf_{(\rho,v,h)\in C(\rho_0,\rho_1)} a^2 \int_0^1 \|h(\cdot,t)\|_1^2 dt + b^2 \int_0^1 \int_\Omega \rho v^2 dxdt$$

where $C(\rho_0,\rho_1)=\{(\rho,v,h),\ \partial_t\rho+\mathrm{div}(\rho v)=h,\ \rho(\cdot,0)=\rho_0,\ \rho(\cdot,1)=\rho_1\}$. Assumptions on the data are essentially identical to the no source term, see eg [17]. They also prove that support localization result for h:

$$\bigcup_{t\in[0,1]}\mathrm{supp}\,h(\cdot,t)\subset\bigcup_{t\in[0,1]}\mathrm{supp}\,\rho(\cdot,t).$$

We remark that this results does not imply finite speed of propagation, that is, as this generalized distance is an interpolation between L^1 and W_2, it is easy to construct examples of initial and final densities for which the interpolation $\rho(\cdot,t)$ has for $t>0$ arbitrarily small a support at a fixed distance from the support of ρ_0. For instance, let us consider the case where ρ_0 and ρ_1 have the same mass, and more precisely, in space dimension 1, with $\Omega=(0,1)$ and $\rho_0(x)=1$ on $(0,\alpha)$ for $\alpha<\frac{1}{2}$, and 0 elsewhere, while $\rho_1(x)=\rho_0(1-x)$. The pure Wasserstein distance is $1-\alpha$. Consider now the pointwise interpolation given by $v=0$, $\rho(x,t)=(1-t)\rho_0(x)+t\rho_1(x)$. This corresponds to $h(x,t)=\rho_1(x)-\rho_0(x)$. Thus

$$a^2\int_0^1\|h(\cdot,t)\|_1^2dt+b^2\int_0^1\int_\Omega\rho v^2dxdt=4a^2\alpha^2.$$

Therefore for a,b such that $4a^2\alpha^2<b^2(1-\alpha)$, the Piccoli-Rossi generalized distance does not give the Wasserstein interpolation for mass balanced densities.

This would somehow bring unphysical results when applied to real images, and one aim of this paper is to provide a generalized distance which recovers the genuine one for balanced densities.

At last, let us mention the user's guide to optimal transportation by Ambrosio-Gigli [1], where the authors present a mass-varying optimal transport initially considered by Figalli and Gigli [11]. Their aim is the following: knowing that the genuine Wasserstein metrics allows to define a solution to the heat equation as the flow of some energy with respect to that metric, the constant mass assumption leads to a Neumann boundary condition for this PDE. A natural question is to wonder how to modify the distance so that the resulting flow is a solution to an heat equation with Dirichlet boundary conditions. This is performed by restricting the transport condition on the interior of the domain, while leaving its boundary without condition. Existence of such a transport plan is proved, as well as properties of the resulting distance. This approach is not a remedy for our application to tumor growth, as far as they are isolated spots on a scanner picture. Indeed in that case, it would be quite unlikely that the growth occurs from a source coming from the boundary.

3. Models of unbalanced mass transport

3.1. General considerations

In this section a generic formulation of unbalanced mass transport is presented and some basic properties are investigated. In what follows, the Eulerian formulation of the optimal mass transport is adopted, that reads:

$$\inf_{(\rho,m)\in C}\left\{\int_0^1\int_\Omega\frac{|m|^2}{2\rho}\,d\Omega dt\right\},\tag{5}$$

$$C=\{(\rho,m)\mid\partial_t\rho+\nabla\cdot m=0,\quad\rho(x,0)=\rho_0,\quad\rho(x,1)=\rho_1\}.\tag{6}$$

One of the basic properties of the optimal transport solution is the invariance with respect to time reflection, *i.e.* $\rho(x,1-t),\mathbf{m}(x,1-t)$ are solution of the problem when ρ_1 is transported in ρ_0. This may be shown by simply considerating the following transformation:

$$x'=x,\tag{7}$$

$$t'=1-t,\tag{8}$$

$$\rho'=\rho,\tag{9}$$

$$m'=-m,\tag{10}$$

$$\lambda'=-\lambda.\tag{11}$$

The action is rewritten by perfoming this change of coordinates:

$$\mathcal{L}'=\int_0^1\int_\Omega\frac{|m'|^2}{2\rho'}+\lambda'(\partial_{t'}\rho'+\nabla_{x'}\cdot m')\,d\Omega'dt,\tag{12}$$

that is formally equivalent to the original action. The change of coordinate leaves the action (and the associated Euler-Lagrange equations) unchanged, so that the solution of the optimal transport will be invariant with respect to this transformation.

Let us consider a generic source term, *i.e.* the constraint will be no longer homogeneous; instead it can be written as:

$$\partial_t \rho + \operatorname{div} m = S(x, t; \rho, m; \rho_0, \rho_1), \tag{13}$$

where S accounts for the mass variation and it may be a function of x, t as well as the variables $(\rho, \mathbf{m})$ and all their derivatives in space and time, the initial and final density (for instance, for normalization purposes).

Among all the possible source terms, it is meaningful to look for those preserving the symmetry property in time that characterizes the classical optimal transport problem. This is done by asking that:

$$S(x, t, \rho, m; \rho_0, \rho_1) = -S(x, 1-t, \rho, -m; \rho_1, \rho_0). \tag{14}$$

Indeed, it may be checked that this condition is sufficient to leave the action unchanged, so that the same argument shown for the balanced case may be adopted. Observe that on the right hand side the initial density is ρ_1 and the final one ρ_0.

As well, a natural condition on S would be to vanish when ρ_0 and ρ_1 have the same mass, so that we recover classical optimal transportation :

$$\left\{ \int_\Omega \rho_0 dx = \int_\Omega \rho_1 dx \right\} \Longrightarrow \{ S(x, t, \rho, m; \rho_0, \rho_1) = 0 \}. \tag{15}$$

The Euler-Lagrange equations associated to the action read:

$$\frac{m}{\rho} - \nabla \lambda - \lambda \frac{\delta S}{\delta m} = 0, \tag{16}$$

$$\partial_t \lambda + \frac{|m|^2}{2\rho^2} + \lambda \frac{\delta S}{\delta \rho} = 0, \tag{17}$$

where δ is the Euler-Lagrange differentiation of the action, that is:

$$\frac{\delta S}{\delta m} = \frac{\partial S}{\partial m} + \sum_{k=1} (-1)^k \nabla^{(k)} \cdot \left(\frac{\partial S}{\partial \nabla^{(k)} m} \right), \tag{18}$$

$$\frac{\delta S}{\delta \rho} = \frac{\partial S}{\partial \rho} + \sum_{k=1} (-1)^k \nabla^{(k)} \cdot \left(\frac{\partial S}{\partial \nabla^{(k)} \rho} \right). \tag{19}$$

$$\tag{20}$$

In the following we will consider several examples of source terms. The affine case amounts to consider a non homogeneous mass conservation, with a constant prescribed source term. While this case is of limited interest for application to real images, we will show that the Benamou-Brenier algorithm easily adapts to that situation. Moreover, for less trivial and time dependent source terms, we will use this algorithm, with an explicit scheme (i.e. by taking the source term at the previous time step).

The first non constant source term we will consider is an exponential model, which is is interesting for modeling the corresponding behavior of tumor growth. We will show explicit solutions for simple cases where the initial and final densities are linked either by a translation/scaling or a affine transformation/scaling.

The second source term considered will somehow use a dual Sobolev norm to estimate the distance between the density pair, by solving a stationary Laplace equation, and use the corresponding flux to drive the mass growth. For that model we will be able to show existence of solution by rephrasing the model as a Monge problem on a manifold and using results of Mc Cann [9].

At last, we will consider a normal growth model where the source term is proportional to the modulus of $\nabla \rho$. While we will not be able to theoretically prove existence on that model, it will turn to be the best choice for the modeling of tumor growth in some situations.

3.2. Remarks on the qualitative behavior of the solutions

In this section some qualitative remarks on the solution nature are proposed. First, it is interesting to investigate whether the solution of an unbalanced optimal transport may be a translation at constant speed and a rescaling, that is:

$$\rho = \rho_0(x - at)\mu(t), \tag{21}$$

where a is a constant vector field (so that $\partial_t a = 0$ and $\nabla a = 0$) and $\mu(t)$ is a scaling factor. In order for the mass conservation equation to be satisfied it is necessary that:

$$S = \partial_t \log(\mu(t))\rho. \tag{22}$$

The Hamilton equation for the lagrange multiplier reduces to:

$$\partial_t \lambda + \frac{|\nabla\lambda|^2}{2} + \partial_t \log(\mu)\lambda = 0. \tag{23}$$

From the Euler-Lagrange equation $a = \nabla\lambda$; hence, by taking the gradient of the Hamilton-Jacobi equation above, the following condition is found:

$$a\partial_t \log(\mu) = 0, \tag{24}$$

that implies that $a = 0$ or $\mu = const$. This means that a pure translation is a solution of a genuine optimal transport problem, a pure scaling is a solution of a differential equation, but a combination of the two can not be solution of an optimal transportation with some source term S. The next paragraph will provide an analytical solution where the translation vector is time varying.

3.2.1. Translation and scaling for an exponential model of growth

Let us look for a particular analytic solution in the case of an exponential source unbalanced optimal transport. Consider an optimal plan between the densities:

$$\rho(x, 0) = \rho_0, \quad \rho(x, 1) = \rho_0(x - a)\exp(c), \tag{25}$$

where a is a constant vector field and $c \in \mathbb{R}$. When an exponential model source is considered, the Euler-Lagrange equations associated to it are:

$$\partial_t \rho + \nabla \cdot (\rho v) = c\rho, \tag{26}$$

$$\partial_t \lambda + \frac{|\nabla\lambda|^2}{2} = -c\lambda. \tag{27}$$

In addition, the velocity is $v = \nabla\lambda$. By taking the gradient of the Hamilton-Jacobi equation, an equation for the velocity is obtained:

$$\partial_t v + v\nabla v = -cv, \tag{28}$$

that means that, if a Lagrangian point of view is assumed:

$$v = \partial_t X(X(\xi)) \;\Rightarrow\; \partial_t X = u_0 \exp(-ct), \tag{29}$$

and, since a solution with a constant translation is sought, namely $X_1 - X_0 = a$,

$$\partial_t X = \frac{c}{1 - \exp(-c)} a \exp(-ct) \;\Rightarrow\; X - X_0 = \frac{1 - \exp(-ct)}{1 - \exp(-c)} a. \tag{30}$$

Let us observe that $X - X_0$ is constant in space. The continuity equation may thus be re-written as:

$$\partial_t \rho + v \cdot \nabla\rho = c\rho, \tag{31}$$

and by introducing $\sigma = \rho\exp(ct)$, this equation reduces to an homogeneous transport equation. The general solution is therefore written as:

$$\rho = \rho_0 \left(x - \frac{1 - \exp(-ct)}{1 - \exp(-c)} a \right) \exp(ct), \tag{32}$$

that verifies the initial and the final conditions as well as the Euler-Lagrange equations. Let us remark that in the limit of a vanishing c, that corresponds to a classical optimal transport, a pure translation is recovered:

$$\lim_{c \to 0} \rho = \rho_0(x - at). \tag{33}$$

3.2.2. Affine mapping: unbalanced homothety

Let us consider the following density pair:

$$\rho(x,0)=\rho_0,\quad \rho(x,1)=\mu\rho_0(Mx),\quad M\in\mathbb{R}^{d\times d},\ \mu\in\mathbb{R}^+, \tag{34}$$

where M is a constant scalar matrix whose entries do not depend upon space and time coordinates and d is the space dimension.

The particular case of an exponential model (see below) is considered, namely:

$$\partial_t\rho+\nabla\cdot(\rho v)=c\rho, \tag{35}$$

$$\partial_t\lambda+\frac{|\nabla\lambda|^2}{2}=-c\lambda. \tag{36}$$

After integration on the space domain of the mass conservation equation, the following relation is obtained:

$$D_t\int_\Omega\rho\ d\Omega=c\int_\Omega\rho\ d\Omega, \tag{37}$$

that, integrated in time between $t=0$ and $t=1$ provides:

$$\int_\Omega\mu\rho_0(Mx)\ dx=\exp(c)\int_\Omega\rho_0\ dx. \tag{38}$$

By performing a change of coordinate in the integral on the left hand side, and by using the fact that the matrix M is given and constant in space, the exponent c may be expressed as function of the determinant of the matrix and the scaling factor μ:

$$c=\ln\left(\frac{\mu}{\det(M)}\right). \tag{39}$$

Let us look for a solution from a lagrangian standpoint:

$$D_tv=-cv\ \Rightarrow\ X(t)=\left(I+\frac{1-\exp(-ct)}{1-\exp(-c)}A\right)\xi, \tag{40}$$

where $(I+A)^{-1}=M$ in order for the final density constraint to be fulfilled.

The velocity field may be expressed from an Eulerian point of view:

$$v(x)=c\frac{\exp(-ct)}{1-\exp(-c)}\left[A\left(I+\frac{1-\exp(-ct)}{1-\exp(-c)}A\right)^{-1}\right]x. \tag{41}$$

Let us define the following matrix:

$$B(t):=\left(I+\frac{1-\exp(-ct)}{1-\exp(-c)}A\right)^{-1}\ \Rightarrow\ B(0)=I,B(1)=M. \tag{42}$$

The backward characteristics may be defined as $Y(x,t)=B(t)x$. It may be checked that $D_tY=0$ and that the velocity may be expressed as:

$$v=\partial_t(B^{-1})Bx=\partial_t(B^{-1})Y=-B^{-1}\partial_tBx. \tag{43}$$

The Eulerian density may be obtained by considering the Jacobian equation written with respect to the backward characteristics:

$$\rho(x,t)=\exp(ct)\rho_0(Y)\det(\nabla_xY), \tag{44}$$

that, after substitution of the expression of Y becomes:

$$\rho(x,t)=\exp(ct)\rho_0(Bx)\det(B), \tag{45}$$

and remark that for $t=0,1$ the constraints on the initial and final densities are recovered.

In the following sections some particular examples of source terms are detailed, that lead to different solution of the unbalanced optimal transport. Their properties will be investigated by means of numerical experiments.

4. Variables independent source: affine constraint

4.1. Formulation

We consider the case where we do not impose (4) anymore. This is particularily relevant in the case where we are interpolating between two images of a growing tumor, for instance. A natural idea is to add a source term in the mass conservation constraint. As this mass growth is supposed to hold on the boundary of domains of homogeneous densities which represents structures in the image, a first guess would be to consider a mass conservation constraint modified like:

$$\partial_t \rho + \operatorname{div}(m) = \alpha \tag{46}$$

where $\alpha : \Omega \times (0, t_m) \to \mathbb{R}$ is given and verifies

$$\int_0^{t_m} \int_\Omega \alpha dx = \int_\Omega \rho_1(x) - \rho_0(x) dx.$$

The simplest form could be to consider is a constant α, which gives:

$$\alpha = \frac{1}{|\Omega| t_m} \int_\Omega \rho_1(x) - \rho_0(x) dx \tag{47}$$

but while it verifies (14)-(15) we will see that this is not the best choice for applications (due to the fact that it is not localized), and therefore we keep a possibly time and space dependant α in the following. The associated Lagrangian is given by

$$L(\phi, \rho, m) = \int_0^{t_m} \int_\Omega \frac{|m|^2}{2\rho} - \rho \partial_t \phi - m \cdot \nabla \phi - \alpha \phi dx dt - \int_\Omega \phi(0, x)\rho_0(x) - \phi(t_m, x)\rho_1(x) dx. \tag{48}$$

Given two densities ρ_0 et ρ_1, the minimization problem is equivalent to the saddle-point problem:

$$\inf_{(\rho,m) \in C_\alpha(\rho_0,\rho_1)} \sup_\phi L(\phi, \rho, m),$$

where

$$C_\alpha(\rho_0, \rho_1) = \{(\rho, v),\ \partial_t \rho + \operatorname{div} m = \alpha,\ \rho(\cdot, 0) = \rho_0,\ \rho(\cdot, t_m) = \rho_1 \text{ on } \Omega,\ m \cdot n = 0 \text{ on } \partial\Omega \times (0, t_m)\}. \tag{49}$$

Arguing as in [4] we introduce dual variables $(a, b) \in \mathbb{R} \times \mathbb{R}^d$ such that

$$\frac{|m|^2}{2\rho} = \sup_{(a,b) \in K} a(t, x)\rho(t, x) + b(t, x) \cdot m(t, x),$$

with

$$K = \left\{ (a, b) : \mathbb{R} \times \mathbb{R}^2 \to \mathbb{R} \times \mathbb{R}^2, \quad a + \frac{1}{2}|b|^2 \leq 0 \text{ on } \mathbb{R} \times \mathbb{R}^2 \right\}.$$

For sake of clarity, we set $\mu = (\rho, m)$ and $q = (a, b)$, and introduce the support function of K, F such that $F(q) = 0$ for $q \in K$ and $F(q) = +\infty$ otherwise. Therefore we have $\frac{|m|^2}{2\rho} = \sup_{q \in K} \mu \cdot q = \sup_q -F(q) + \mu \cdot q$. At last we set

$$G(\phi) = \int_\Omega \phi(0, x)\rho_0(x) - \phi(t_m, x)\rho_1(x) dx.$$

Still following [4], we show that our saddle point problem can be written as

$$\sup_\mu \inf_{\phi, q} F(q) + G(\phi) + \langle \mu, \nabla_{t,x} \phi - q \rangle + \langle \alpha, \phi \rangle, \tag{50}$$

where the brackets stand for the $L^2(Q_m)$ scalar product, the variables μ, q are taken in $L^2(Q_m)^{d+1}$, and ϕ in $H^1(Q_m)$. We now aim at finding a saddle-point of this problem which corresponds to a standard form of [12] in order to apply augmented Lagrangian techniques. The formal optimal condition for this problem are:

$$\begin{cases} \partial_t \phi + \frac{|m|^2}{2\rho^2} = 0 & \text{in } [0,t_m]\times\Omega \\ \partial_t \rho + \operatorname{div} m = \alpha & \text{in } [0,t_m]\times\Omega \\ \frac{m}{\rho} = \nabla\phi & \text{in } [0,t_m]\times\Omega \\ \rho(0,.) = \rho_0 & \text{in } \Omega \\ \rho(t_m,.) = \rho_1 & \text{in } \Omega \end{cases}$$

Observing that the variable m can be eliminated, the optimality conditions can be rewritten in term of ρ, ϕ and c as:

$$\begin{cases} \partial_t \phi + \frac{|\nabla\phi|^2}{2} = 0 & \text{in } [0,t_m]\times\Omega \\ \partial_t \rho + \operatorname{div}(m) = \alpha & \text{in } [0,t_m]\times\Omega \\ \rho(0,.) = \rho_0 & \text{in } \Omega \\ \rho(t_m,.) = \rho_1 & \text{in } \Omega \end{cases} \tag{51}$$

Therefore the optimal mass transfer still follows straight lines. We then define the augmented Lagrangian by introducing $r > 0$:

$$L_r(\phi,q,\mu) = F(q) + G(\phi) + \langle \mu, \nabla_{t,x}\phi - q\rangle + \langle \alpha,\phi\rangle + \frac{r}{2}\left\langle \nabla_{t,x}\phi - q, \nabla_{t,x}\phi - q\right\rangle. \tag{52}$$

4.2. Algorithm

We consider the following iterative algorithm to compute this saddle point numerically: This algorithm builds from $(\phi^{n-1}, q^{n-1}, \mu^n, c^{n-1})$ the next iterate, and is very close to the original Benamou-Brenier algorithm. We just describe the differences in the three steps.

Step A $\phi^n = \arg\min L_r(\,.\,, q^{n-1}, \mu^n)$ This still amounts to solve a Poisson equation, but now with an extra contribution coming from α. Namely, taking the differential with respect to ϕ gives

$$G(\phi) + \langle \mu^n, \nabla_{x,t}\phi\rangle + \langle \alpha,\phi\rangle + r\left\langle \nabla_{x,t}\phi^n - q^{n-1}, \nabla_{x,t}\phi\right\rangle = 0, \qquad \forall \phi$$

which, for Dirichlet boundary conditions gives, following [3]:

$$-r\Delta_{x,t}\phi^n = \operatorname{div}_{x,t}(\mu^n - rq^{n-1}) - \alpha \qquad (x,t)\in\Omega\times]0,t_m[$$

with non homogeneous Neumann boundary conditions in space and time:

$$r\partial_t\phi^n(x,0) = \rho_0(x) - \rho^n(0,x) + ra^{n-1}(x,0) \qquad r\partial_t\phi^n(x,t_m) = \rho_1(x) - \rho^n(t_m,x) + ra^{n-1}(t_m,x) \tag{53}$$

$$r\partial_n\phi^n(x,t) = rb^{n-1}(x)\cdot n - m^n\cdot n \quad \text{on } \partial\Omega\times(0,t_m) \tag{54}$$

Step B $q^n = \arg\min L_r(\phi^n, \,.\,, \mu^n)$ is identical to [3], i.e. a pointwise projection on a paraboloid.
Step C $\mu^{n+1} = \arg\max L_r(\phi^n, q^n, \,.\,)$ is identical to [3].

5. Source proportional to a scalar field

In this section another source model is investigated of the form:

$$S(x,t;\rho,m;\rho_0,\rho_1) = -\rho\partial_t\Gamma - m\cdot\nabla\Gamma = -\rho D_t\Gamma, \tag{55}$$

where $\Gamma(x,t)$ is a given scalar field and D_t is the total (lagrangian) derivative. Two different cases will be investigated: an exponential type of growth and a heat flux guided growth.

5.1. Exponential model of growth

5.1.1. Introduction

For this first model, let us consider a source of the form:

$$S = -c\rho \tag{56}$$

where $c \in \mathbb{R}$ is a constant. Integrating $\partial_t \rho + \operatorname{div} m = -c\rho$ in space gives, using the homogeneous boundary conditions on m,

$$\frac{d}{dt}\int_\Omega \rho dx = -c\int_\Omega \rho dx. \tag{57}$$

The expression for c may be computed *a priori*, depending only on the initial and the final mass only. Indeed upon integration of the first order ODE (57) we get:

$$c = \frac{1}{t_m}\log\left(\frac{\int_\Omega \rho_0\ dx}{\int_\Omega \rho_1\ dx}\right). \tag{58}$$

Note that the source term (56) with c given by (58) verifies (14)-(15). Another way to derive an expression for c is to integrate both members of (57), and this leads to a growth rate which depends nonlinearly on ρ:

$$c[\rho] = \frac{\int_\Omega \rho_0 - \rho_1\ dx}{\int_0^{t_m}\int_\Omega \rho\ dx}. \tag{59}$$

One could wonder whether the linear growth model and the nonlinear one would give the same optimal path, if it exists. We have equivalence of these two models of growth:

Proposition 1. *Let $\rho_0, \rho_1 \in L^1(\Omega)$ be nonnegative, with positive integrals on Ω, and define the sets*

$$C_1 = \Bigg\{(\rho, m) \in L^1((0,t_m)\times\Omega)\times L^1(0,t_m;W^{1,1}(\Omega)),\quad \partial_t\rho + \operatorname{div} m = -c\rho,\ c = \frac{1}{t_m}\log\left(\frac{\int_\Omega \rho_0\ dx}{\int_\Omega \rho_1\ dx}\right)$$
$$\rho(\cdot,0) = \rho_0,\ \rho(\cdot,t_m) = \rho_1,\ m\cdot n = 0 \text{ on } \partial\Omega\times(0,t_m)\Bigg\} \tag{60}$$

and

$$C_2 = \Bigg\{(\rho, m) \in L^1((0,t_m)\times\Omega)\times L^1(0,t_m;W^{1,1}(\Omega)),\quad \partial_t\rho + \operatorname{div} m = -c[\rho]\rho,\ c[\rho] = \frac{\int_\Omega \rho_0 - \rho_1\ dx}{\int_0^{t_m}\int_\Omega \rho\ dx}$$
$$\rho(\cdot,0) = \rho_0,\ \rho(\cdot,t_m) = \rho_1,\ m\cdot n = 0 \text{ on } \partial\Omega\times(0,t_m)\Bigg\} \tag{61}$$

Assume $C_1 \neq \emptyset$. Then $C_1 = C_2$.

Proof. Let $(\rho, m) \in C_1$. From the positiveness of the integrals of initial and final densities, integrating (57) from 0 to t and from t to t_m for $t \in (0, t_m)$ gives (assuming $c \leq 0$ without loss of generality):

$$0 < \int_\Omega \rho_0 dx \leq \int_\Omega \rho(x,t)dx \leq \int_\Omega \rho_1 dx \qquad \text{on } (0,t_m).$$

Therefore we can compute $c[\rho]$ as above and find $c[\rho] = c$, thus $(\rho, m) \in C_2$, which is nonempty. Now take $(\rho, m) \in C_2$, $c[\rho]$ is a constant and integrating the ODE (57) give $c[\rho] = c$, thus $(\rho, m) \in C_1$. □

5.1.2. Existence and uniqueness of the solution

Let us investigate the existence and uniqueness of the solution. Consider two densities ρ_0, ρ_1 such that $\rho_0 \neq \rho_1\exp(-c)$. Let us introduce a new variable $\sigma = \rho\exp(ct)$. This change of variable leads to an homogeneous mass constraint for σ. The problem lagrangian action may be rewritten as:

$$\mathcal{L}(\sigma, v) = \int_0^1\int_\Omega \frac{1}{2}\sigma\exp(-ct)v^2 + \phi(\partial_t\sigma + \nabla\cdot(\sigma v))\ d\Omega\ dt. \tag{62}$$

This is an optimal transport problem with a scalar metric that depends upon time. It may be recast in lagrangian coordinates $(X(\xi,t) \mid X(\xi,0)=\xi$ and velocity $v(X(\xi,t),t) := \dot{X}(\xi,t))$ as:

$$\mathcal{L}(X) = \int_0^1 \int_{\Omega_0} \frac{1}{2}\sigma_0(\xi)\exp(-ct)\dot{X}^2 + \psi(\xi)(\sigma_0(\xi) - \sigma(X)\det(\nabla_\xi X))\ d\Omega_0\ dt. \tag{63}$$

For the Jensen inequality, it holds:

$$\int_0^1 \int_{\Omega_0} \frac{1}{2}\sigma_0(\xi)\exp(-ct)\dot{X}^2\ d\Omega_0\ dt \geq \int_{\Omega_0} \frac{1}{2}\sigma_0(\xi)d^2(\xi,X(\xi))\ d\Omega_0, \tag{64}$$

where $d^2(\xi,X)$ is the geodesic distance squared between ξ and $X(\xi)$. Let us prove that the equality holds for a velocity field $v=\dot{X}$ which is related to the solution of the optimal transportation problem between σ_0 and σ_1.

Proposition 2. *The geodesics are straight lines and the geodesic distance is proportional to the euclidean distance between the extrema.*

Proof. Consider $\gamma : [0,1] \to \mathbb{R}^d$. This curve is a geodesics if:

$$\gamma(t) = \arg\min_{\tilde{\gamma}} \int_0^1 \exp(-ct)|\dot{\tilde{\gamma}}|^2\ dt, \tag{65}$$

whose integration between $\gamma(0)=\xi$ and $\gamma(1)=X$ leads to:

$$\gamma(t) = \frac{\exp(c)}{\exp(c)-1}\xi - \frac{1}{\exp(c)-1}X + \frac{\exp(ct)}{\exp(c)-1}(X-\xi), \tag{66}$$

which is a straight line with non-constant speed. The geodesic distance is computed by inserting the time derivative of the curve into the expression of the distance, providing:

$$d(\xi,X)^2 = \frac{c}{\exp(c)-1}|X-\xi|^2, \tag{67}$$

that completes the proof. Observe that in the limit of vanishing c, the euclidean distance is recovered and the straight lines are parametrized at constant speed. □

By using the result of this proposition, the expression of the velocity $v=\dot{X}$ may be derived.

Indeed, the minimizer of the geodesic distance under the lagrangian mass constraint satisfies:

$$X = \arg\min_{\tilde{X}\in C} \int_{\Omega_0} \frac{1}{2}\sigma_0(\xi)d^2(\xi,X(\xi))\ d\Omega_0 = \arg\min_{\tilde{X}\in C} \frac{c}{\exp(c)-1}\int_{\Omega_0} \frac{1}{2}\sigma_0(\xi)|X-\xi|^2\ d\Omega_0, \tag{68}$$

$$C = \{X | \sigma_0(\xi) = \sigma_1(X(\xi)\det(\nabla_\xi X))\}. \tag{69}$$

The solution is a classical optimal transport between σ_0 and σ_1. There exists a unique minimizer and $X(\xi,1) = \xi + \nabla_\xi\Phi$, where $\frac{\xi^2}{2} + \Phi(\xi)$ is a convex function.

This solution is parametrized at non-constant speed for the time mapping $X(\xi,t)$ to be geodesic:

$$X(\xi,t) = \xi + \frac{(\exp(ct)-1)}{\exp(c)-1}\nabla_\xi\Phi \quad \Rightarrow \quad v = \dot{X} = \frac{c\exp(ct)}{\exp(c)-1}\nabla_\xi\Phi. \tag{70}$$

The expression of the velocity is introduced into the Eq.(64) and the following holds:

$$\min_{\dot{X}} \int_0^1 \int_\Omega \frac{1}{2}\exp(-ct)\sigma_0\dot{X}^2\ d\Omega_0\ dt = \min_X \int_{\Omega_0} \frac{1}{2}\sigma_0 d^2(\xi,X)\ d\Omega_0 = \frac{1}{2}\frac{c}{\exp(c)-1}W^2(\sigma_0,\sigma_1), \tag{71}$$

where $\dot{X}$ is chosen as in Eq.(70). Thus, the problem of minimizing the action in Eq.(62) admits an unique solution.

5.2. Heat flux guided model

The counterpart of the exponential model of growth consists in taking $S = -m \cdot \nabla\Gamma(x)$, where Γ may be either a given field depending upon some known information associated to the problem, or a quantity to be determined as function of the problem data (*i.e.* ρ_0, ρ_1) in order to set up a parametric free model. A perspective on the modeling of constraints by using mass sources is presented below.

A preliminary constraint on Γ is derived. Let us introduce the density $\sigma := \rho \exp(\Gamma(x))$. Hence:

$$\partial_t \rho + \nabla \cdot \rho v + m \cdot \nabla\Gamma = 0 \;\Rightarrow\; \partial_t \sigma + \nabla \cdot (\sigma v) = 0, \tag{72}$$

so that σ satisfies an homogeneous constraint. This imply:

$$\int_\Omega \sigma(x,0)\; d\Omega = \int_\Omega \sigma(x,1)\; d\Omega \quad \Rightarrow \quad \int_\Omega (\rho_1 - \rho_0) \exp(\Gamma)\; d\Omega = 0, \tag{73}$$

the exponential of the source Γ is orthogonal to the density difference with respect to the L_2 scalar product.

Among all the possible ways to define the function Γ, a heat-like solution is adopted.

The source Γ is the solution of:

$$(\Gamma^*, \mu^*) = \arg \inf_\Gamma \sup_\mu \int_\Omega \frac{1}{2}|\nabla\Gamma|^2 - \frac{|\delta M|}{\delta M}\Delta\rho\Gamma\; d\Omega - \mu \int_\Omega \Delta\rho \exp(\Gamma), \tag{74}$$

where the scalar μ is the lagrange multiplier enforcing the orthogonality constraint. Homogeneous Dirichlet boundary conditions are used for Γ.

The Euler-Lagrange equations reads:

$$-\nabla^2\Gamma = \left(\frac{|\delta M|}{\delta M} + \mu \exp(\Gamma)\right)\Delta\rho, \quad \text{in } \Omega, \tag{75}$$

$$\Gamma = 0, \quad \text{on } \partial\Omega, \tag{76}$$

$$\int_\Omega \Delta\rho \exp\Gamma\; d\Omega = 0. \tag{77}$$

The problem is solved by an Uzawa augmented lagrangian method, the starting value adopted for the lagrangian multiplier μ being $\mu = 0$.

Some properties of the solution of this system are highlighted.

When $\delta M = 0$, that is when the initial and final densities have the same mass, $\Gamma = 0$, identically, and a classical optimal transport is recovered.

To verify that the time-reversal symmetry of optimal transport is satisfied, the following transformation is applied to the solution of the system:

$$\Delta\rho' = -\Delta\rho \tag{78}$$

$$\mu' = -\mu'. \tag{79}$$

From the first transformation, the sign of δM changes and the following is obtained:

$$-\nabla^2\Gamma' = \left(-\frac{|\delta M|}{\delta M} - \mu \exp(\Gamma')\right)(-\Delta\rho), \quad \text{in } \Omega, \tag{80}$$

$$\Gamma' = 0, \quad \text{on } \partial\Omega, \tag{81}$$

so that $\Gamma' = \Gamma$ and the time reversal symmetry is preserved.

The boundary integral of the normal derivative of Γ is related to the absolute value of the mass difference between the densities. Indeed, the integral over the whole domain of the solution leads to:

$$-\int_{\partial\Omega} \partial_n\Gamma\; dS = |\delta M|. \tag{82}$$

Note that the source Γ encodes the distance between the supports of the densities (it is related to the H^{-1} distance between them) and the mass difference.

5.2.1. Existence and uniqueness of the solution

As seen in Eq.(72) it is possible to rewrite this model through a change of variables in such a way that the constraint, in the new variables, is the classical homogeneous one. The action, in the new variables, may be written as:

$$\mathcal{L}(\sigma, v) = \int_0^1 \int_\Omega \frac{1}{2}\sigma \exp(-\Gamma)v^2 + \phi(\partial_t \sigma + \nabla \cdot (\sigma v))\ d\Omega\ dt, \tag{83}$$

which is an homogeneous transport with a scalar metric factor $\exp(-\Gamma)$. Let us remark that in the case of balanced densities $\Gamma = 0$ and the classical optimal transportation problem in Benamou-Brenier formulation is recovered.

The existence and uniqueness of the solution of this non-classical optimal transportation problem is investigated by first showing that this problem can be formulated as a Monge optimal transport problem on a manifold. Let us introduce the lagrangian coordinate $X(\xi, t) \mid X(\xi, 0) = \xi$. The velocity $v(X(\xi, t), t) := \dot{X}(\xi, t)$. Thus:

$$\mathcal{L}(X) = \int_0^1 \int_{\Omega_0} \frac{1}{2}\sigma(X) \exp(-\Gamma(X))\dot{X}^2 + \psi(\xi)(\sigma_0(\xi) - \sigma(X) \det(\nabla_\xi X)) \det(\nabla_\xi X)\ d\Omega_0\ dt. \tag{84}$$

By applying the mass conservation equation in Lagrangian form, the time integral of the kinetic energy transforms into:

$$\mathcal{K}(X) = \int_0^1 \int_{\Omega_0} \frac{1}{2}\sigma_0(\xi) \exp(-\Gamma(X))\dot{X}^2\ d\Omega_0\ dt \tag{85}$$

This case may be considered as an optimal transportation on a Riemannian manifold, whose metric tensor is $g_{ij} = \exp(-\Gamma(X))\delta_{ij}$. Let us restrict to the strong solutions of Eq.(**??**), so that $\Gamma \in C^2(\Omega)$. This is a sufficient condition for the manifold to be C^3 smooth, *i.e.* for the metric tensor to be twice continuously differentiable. Thus, by applying the results of [9], the solution of this problem exists unique.

Moreover, Jensen inequality leads to:

$$\int_0^1 \int_{\Omega_0} \frac{1}{2}\sigma_0(\xi) \exp(-\Gamma(X))\dot{X}^2\ d\Omega_0\ dt \geq \int_{\Omega_0} \frac{1}{2}\sigma_0(\xi) d^2(\xi, X)\ d\Omega_0, \tag{86}$$

where d is the geodesic distance on the manifold and X is such that $\sigma_0(\xi)$ is mapped into $\sigma_1(X(\xi))$ by the exponential map on the manifold (see [9] for more details).

6. Source proportional to the modulus of the density gradient: nonlinear constraint

Another formulation for the source term would be to introduce some nonlinear growth term in α, which leads to a normal growth. We propose the following form:

$$\alpha = \beta|\nabla\rho|, \quad \text{where } \beta = \frac{\int_\Omega \rho_1 - \rho_0 dx}{\int_0^{t_m} \int_\Omega |\nabla\rho| dx}. \tag{87}$$

This choice is justified as follows: it merely says that mass variation is more localized on regions where ρ is varying. This seems natural to see a growing set as gaining mass on the boundary. The β term ensures that the gain of mass is compatible with the difference of mass between initial and final densities. The corresponding set of constraints

$$C_\alpha(\rho_0, \rho_1) = \Bigg\{ (\rho, v),\ \partial_t \rho + \operatorname{div} m = \frac{\int_\Omega \rho_1 - \rho_0 dx}{\int_0^{t_m} \int_\Omega |\nabla\rho| dx} |\nabla\rho|, \\ \rho(\cdot, 0) = \rho_0,\ \rho(\cdot, t_m) = \rho_1 \text{ on } \Omega,\ m \cdot n = 0 \text{ on } \partial\Omega \times (0, t_m) \Bigg\}. \tag{88}$$

seems not easy to deal with numerically. However, in the context of our augmented Lagrangian approach, we can use a quasi-static formulation which, at each iteration, amounts to use for α its expression in terms of ρ^n. This means that our algorithm reduces to the original Benamou-Brenier algorithm where we just change step 1 to the

Nonlinear step 1 $\phi^n = \arg\min L_r(\,.\,, q^{n-1}, \mu^n)$ which amounts to solve the Poisson equation,

$$-r\Delta_{x,t}\phi^n = \mathrm{div}_{x,t}(\mu^n - rq^{n-1}) - \frac{\int_\Omega \rho_1 - \rho_0 dx}{\int_0^{t_m}\int_\Omega |\nabla\rho^n| dx}|\nabla\rho^n| \qquad (x,t)\in\Omega\times]0,t_m[$$

with the same non homogeneous Neumann boundary conditions in space and time.

7. Numerical tests

Mass variations can manifest in different ways, we investigate first the case where two images have same maxima but still different mass. For instance consider the case where:

$$\rho_0(x,y) = e^{-300\left(\frac{(x-0.3N)^2}{N^2}+\frac{(y-0.7N)^2}{2N^2}\right)}, \quad \rho_1(x,y) = e^{-200\left(\frac{(x-0.7N)^2}{2N^2}+\frac{(y-0.3N)^2}{N^2}\right)}$$

where $N\times N$ is image size, we took $N = 64$ in the our tests. Note that the iso-contours are ellipses, of different orientations. We plot in figure 1 some pictures on the optimal path obtained with the exponential source term, and on figure 2(a) the mass variation during the corresponding interpolation. On figure 2(b) we depicted the

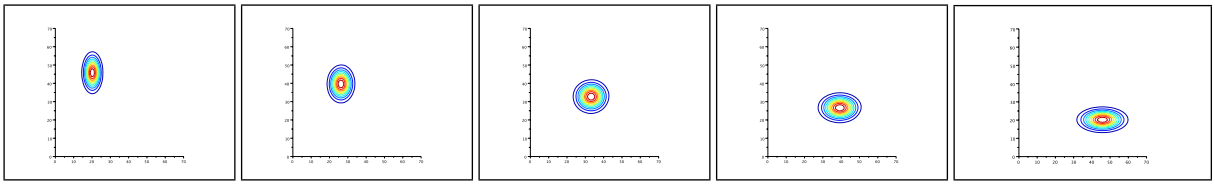

FIG 1. *Plot of the isolevels of the density $\rho(t)$ along the optimal path between two densities of different mass.*

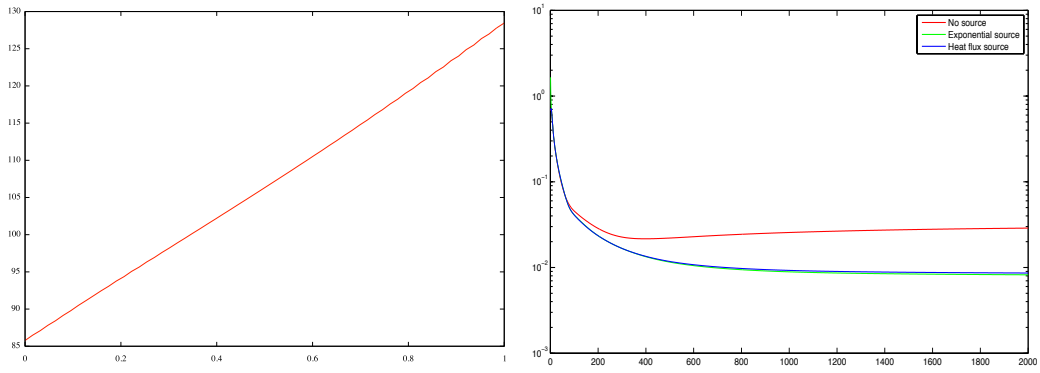

FIG 2. *(a) Plot of the mass variation from initial to final density during the optimal path for the exponential source term. (b) Plot of the residual variation during iterations, for the no-source, exponential source, and heat flux source algorithms. Note that the vertical axis is log-scaled.*

residual decrease (in log scale) versus iterations, for the genuine no-source algorithm, the exponential and heat flux algorithms that we introduced. Note that the exponential algorithm performs very well, with a decreasing residual, on contrary with the no-source algorithm (that is beyond the domain of its validity, by the way). Another test consists in keeping the same support but consider different magnitudes. This is the case for the following initial and final densities, whose iso-contours are circles.

$$\rho_0(x,y) = 1.5e^{-300\left(\frac{(x-0.3N)^2}{N^2}+\frac{(x-0.7N)^2}{N^2}\right)}, \quad \rho_1(x,y) = e^{-300\left(\frac{(x-0.7N)^2}{N^2}+\frac{(x-0.3N)^2}{N^2}\right)}.$$

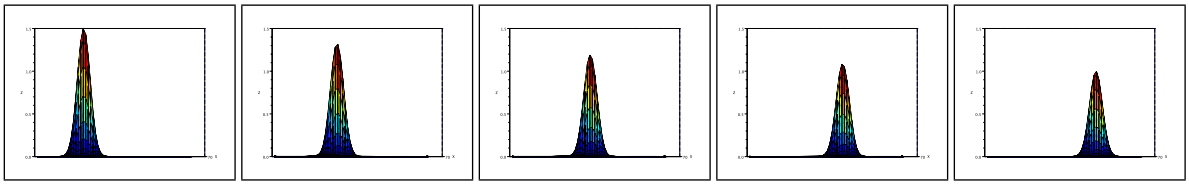

FIG 3. *Plot of the isolevels of the density $\rho(t)$ along the optimal path between two densities of different mass.*

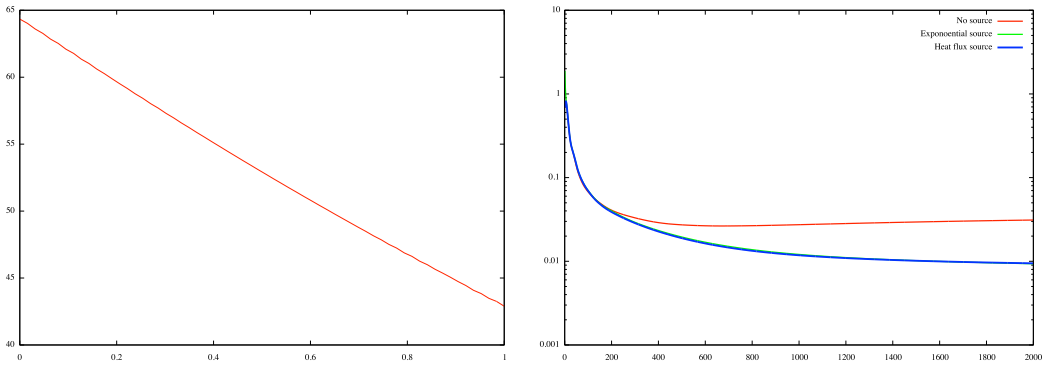

FIG 4. *(a) Plot of the mass variation from initial to final density during the optimal path of the exponential source term. (b) Plot of the residual variation during iterations, for the no-source, exponential source, and heat flux source algorithms. Note that the vertical axis is log-scaled.*

As this is a symmetrical case, we depicted a side view on figure 3 to show the maximum decreasing, and in figure 4(a) the mass variation as well, still using our exponential source term. In figure 4(b) we plotted the residual decrease, and note that the exponential and heat flux source terms gave nearly the same decrease in that case.

Note that in both cases, the optimal path is symmetric, that is, interpolating from ρ_0 to ρ_1 or from ρ_1 to ρ_0 gives the interpolating densities which are equal upon the transformation of t to $1 - t$.

Next, we will consider the more intricate case where a mass splitting occurs. This could be relevant in tumor or more generally in cell growth. Our toy example corresponds to an initial gaussian function defined by

$$\rho_0(x, y) = e^{-200\left(\frac{(x-0.5N)^2}{N^2} + \frac{(x-0.2N)^2}{N^2}\right)}$$

which is supposed to be transported onto

$$\rho_1(x, y) = 4e^{-200\left(\frac{(x-0.25N)^2}{N^2} + \frac{(x-0.8N)^2}{N^2}\right)} + e^{-200\left(\frac{(x-0.75N)^2}{N^2} + \frac{(x-0.8N)^2}{N^2}\right)}.$$

As is clearly seen from figure 5, the genuine Benamou-Brenier algorithm attempts to create an optimal pas by adding mass at the very end of the path, while our algorithm produces a smooth mass variation which is more what we could expect form the interpolation of these two unbalanced densities.

7.1. Non-rigid registration for a growing lung metastasis

In this section some numerical tests on the non-rigid registration in biomedical imagery is proposed. Registration is adopted to refer to the same geometric configuration, especially when highly deformable organs are considered. The optimal transport is an objective way to provide a geometric transformation to this end. However, when tissue is evolving, as in tumor growth, the mass (measured considering the grey scale intensity) is not constant and a simple renormalization may provide unphysical mappings. A more accurate transformation could be obtained by considering continuous models of tumor growth. These models are often parametric and need

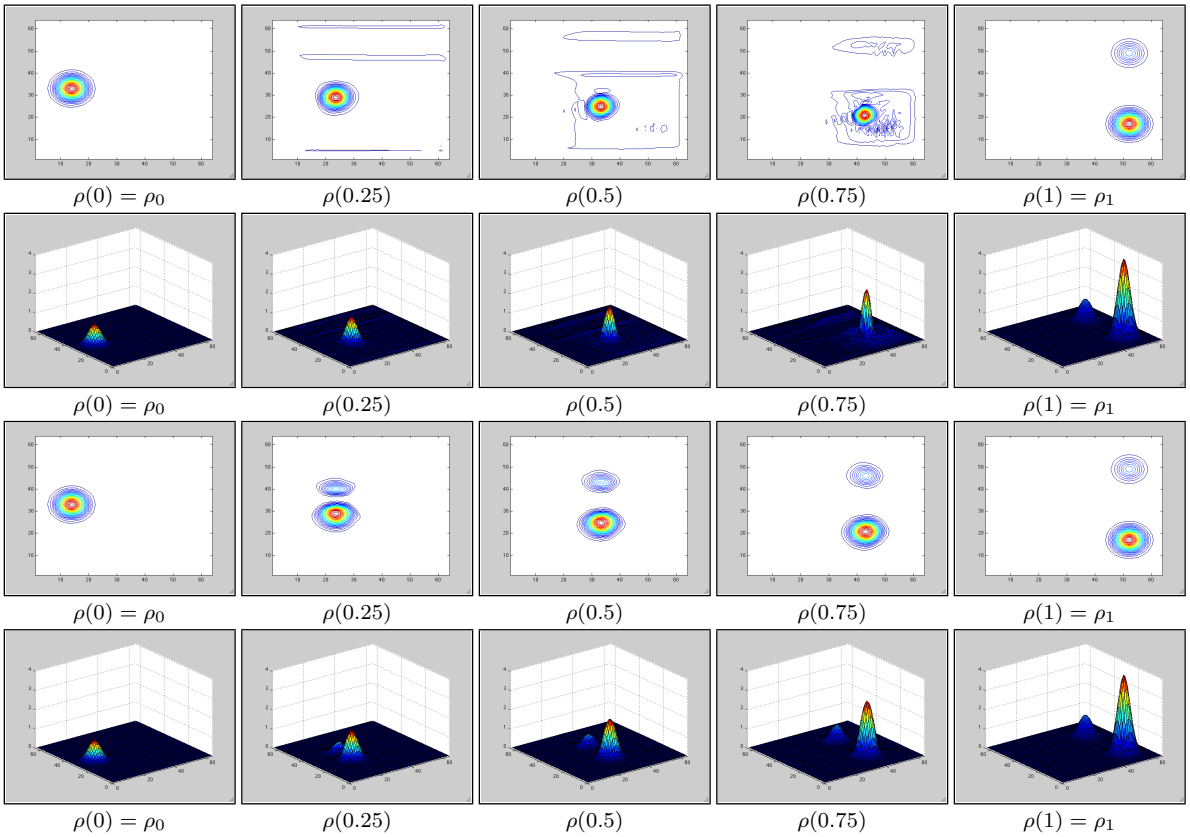

FIG 5. *Plot of the isolevels of the density $\rho(t)$ along the optimal path between two densities of different mass. Top rows: original Benamou-Brenier Algorithm, with top and side views; Bottom rows: Our algorithm with exponential source term.*

a calibration, which may result in a costly process from a computational stand point. If the aim is not to investigate tumor growth dynamics but just to obtain a geometrical transformation, the proposed algorithms may be adopted.

The numerical experiments described hereafter concerns the non-rigid registration of portions of lung tissue with metastatic nodules. Several cases are considered, corresponding to different behaviors of the tumor growth.

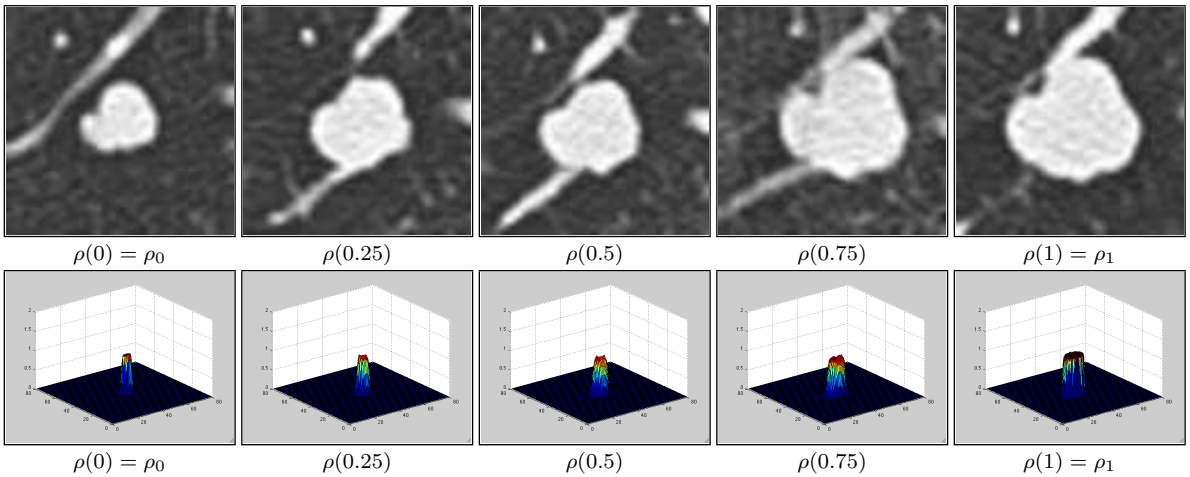

FIG 6. *Plot of a growing tumor simulation from an initial and final stage. Top: B/W images; Bottom: corresponding density plots.*

The first case considered is a sequence of 5 CT scan, shown in Fig.6. They are a 2D slice of a 3D CT scan, represented in grey scale. The original images were segmented by using a simple threshold method. The three

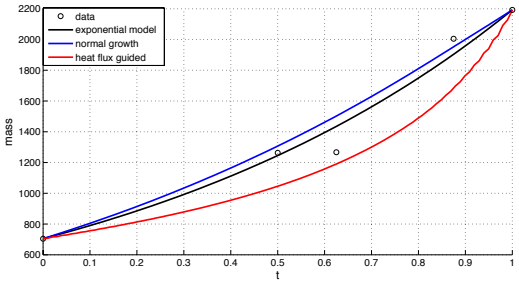

FIG 7. *Mass curve as function of time for different source models (color continuous line), compared to the data (black circles).*

model of source that we proposed were tested by taking the first and the last image of the sequence as initial and final densities respectively. In Fig.7 the mass curve are compared to the real data: black circles are the masses of the segmented images, the black line is the mass of the interpolation obtained by an exponential source, the blue and the red one are the mass curves for the normal growth and the heat flux guided model. The real time scale for this evolution is 45 months: for the present work the time has been renormalized to $[0, 1]$; the same choice has been performed for all the testcases. The growth, in this case, is rather complex. Let us remark that the data are affected by noise and large errors may occur in the evaluation of the mass of the images after segmentation (even 30-40% of uncertainty). The three model proposed behaved differently and, despite the lack of biological modeling, the exponential and the normal sources are able to render the overall mass evolution with an error that is high but not larger than the measurement error, in some cases. The same considerations hold true for all the subsequent cases. In Fig.(8-10) the comparison between the interpolation

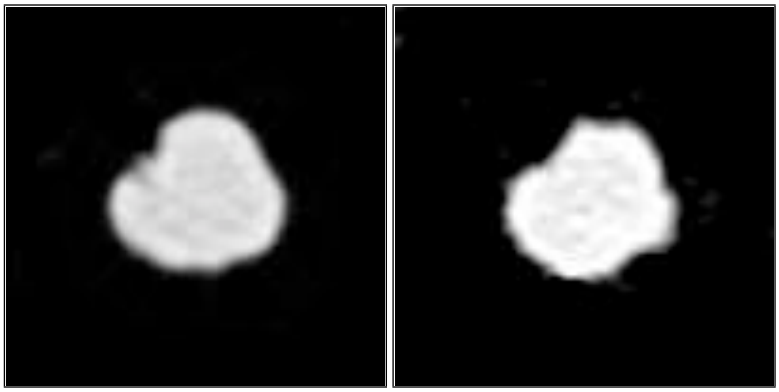

a) $\rho(0.25)$ b) $\overline{\rho}(0.25)$

FIG 8. *Comparison between the interpolation at time $t = 0.5$, a), obtained by solving optimal transport between images $(1-5)$ and the original image in grey scale b)*

and the real data is shown,when the exponential model of growth is used. The images appears more regular in terms of shape with respect to the original one, but the accordance is good. In Fig. 9 the interpolated image is featured by a larger mass than the datum, and the error is at its maximum (as it can be checked by looking at Fig.7).

7.1.1. Fast super-exponential growth

The second case we considered is a fast growth. A tissue portion is considered, in which a lung metastasis is growing. In Fig.7.1.1 the sequence of three realistic images is shown. We tested three different model of sources, namely the exponential growth, the non-linear normal model and the heat-guided flux model. In particular, the

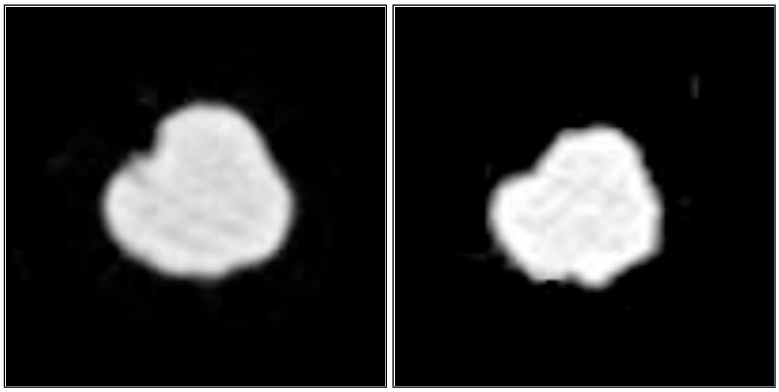

a) $\rho(0.50)$ b) $\overline{\rho}(0.50)$

FIG 9. *Comparison between the interpolation at time $t = 0.625$, a), obtained by solving optimal transport between images $(1-5)$ and the original image in grey scale b)*

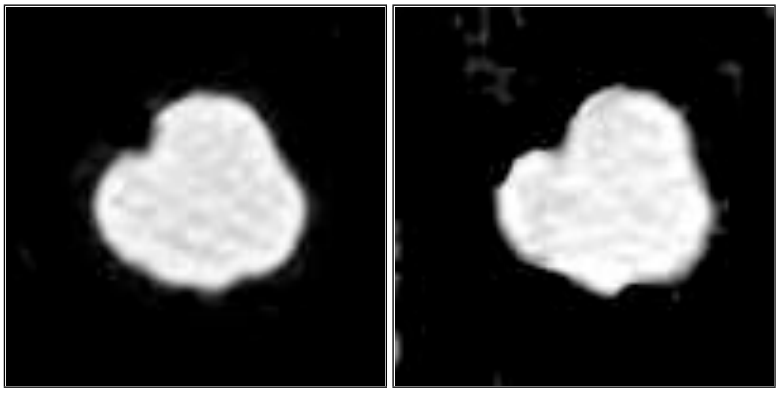

a) $\rho(0.75)$ b) $\overline{\rho}(0.75)$

FIG 10. *Comparison between the interpolation at time $t = 0.875$, a), obtained by solving optimal transport between images $(1-5)$ and the original image in grey scale b)*

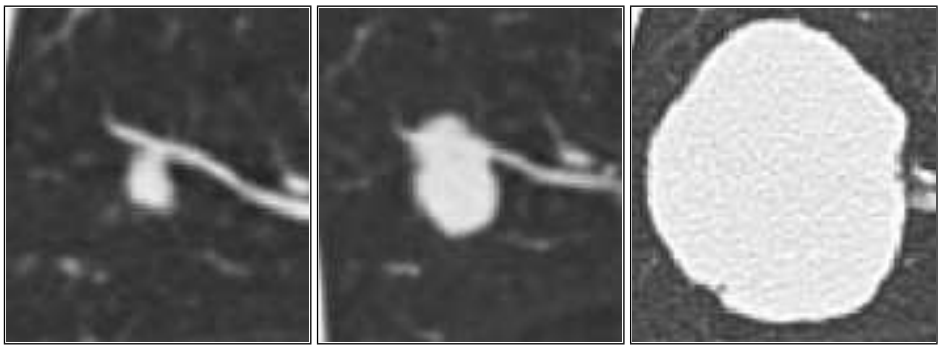

$\rho(0) = \rho_0$ $\rho(0.5)$ $\rho(1.0) = \rho_1$

optimal transport between the first and the last image was computed. In Fig.11 the mass curve as function of time is shown for the three model sources compared to the data. There is a considerable increase of the tumor mass (about 6000%), that makes this case particularly challenging. For this case, the exponential source model was the more accurate one from a quantitative point of view (compare the three curves with the datum available at $t = 0.5$).

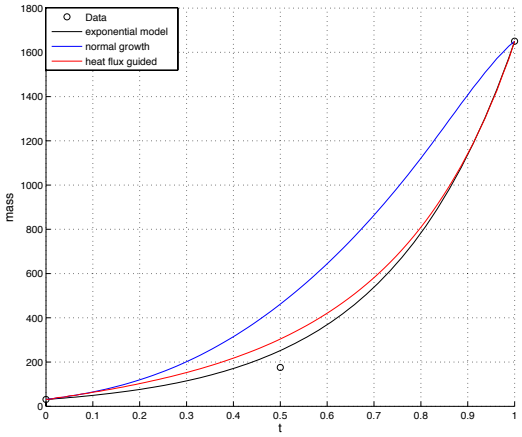

FIG 11. *Mass curve as function of time for different source models (color continuous line), compared to the data (black circles).*

7.1.2. Logistic-type growth

The last case we considered is a tumor which initially grows in a rapid way and then undergoes a plateau type of evolution. The same analysis done for the previous cases is performed. In Fig.12 the mass curve is shown

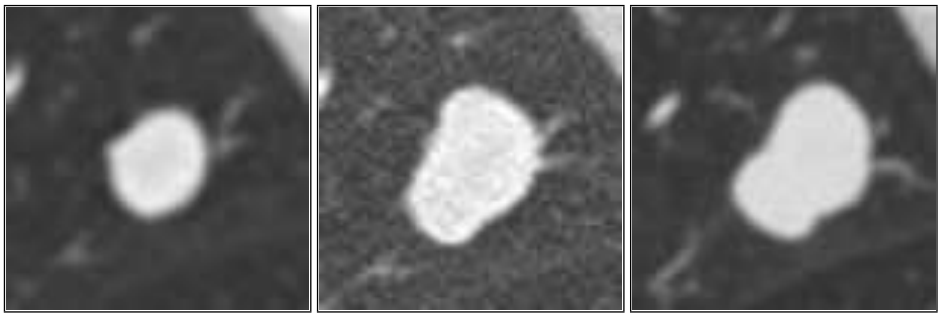

$\rho(0) = \rho_0$ $\rho(0.5)$ $\rho(1.0) = \rho_1$

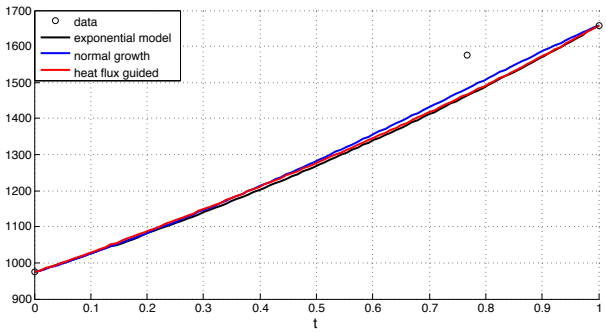

FIG 12. *Mass curve as function of time for different source models (color continuous line), compared to the data (black circles).*

for the different source models. The three models behave quite similarly in this case, and the more accurate one, that is, the one which is closer, in terms of mass, to the intermediate datum, is the normal growth one (blue curve in Fig.12). None of the models is able to render a plateau-type of solution. A perspective might concern the setting up of a logistic model source to deal with this kind of growth. After having investigated the

mass properties, the interpolation of the image is checked. In Fig.13 the comparison between the interpolated

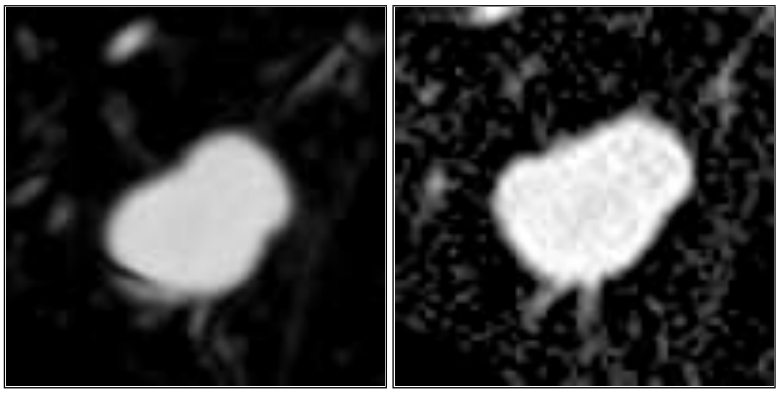

a) $\rho(0.8)$ b) $\overline{\rho}(0.8)$

FIG 13. *Comparison between the interpolation at time $t = 0.8$, a), obtained by solving optimal transport between images $(1-3)$ and the original image in grey scale b)*

and the original image is shown. The tumor dimension as well as the main features of the tissue configuration are qualitatively well represented. The models proposed provide quite a good interpolation of tissues evolution, albeit their simplicity and the fact that they disregard the biology that governs the phenomena involved.

7.2. Morphogenesis of kidneys

In this subsection a biological tree growth is considered. Several realistic images of the branching process occurring in the kidneys morphogenesis are available. As for the tumor growth case, there is no aim in investigating or understanding the biological and biophysical phenomena involved, but a realistic interpolation is sought. In

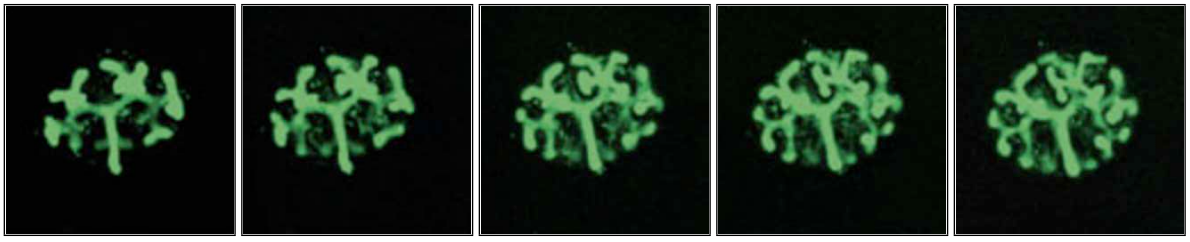

$\rho(0) = \rho_0$ $\rho(0.25)$ $\rho(0.5)$ $\rho(0.75)$ $\rho(1) = \rho_1$

FIG 14. *Images of kidneys morphogenesis*

Fig.14 a sequence of five realistic images is shown. The main limitation and error source is related to the fact that they are 2D projections of a 3D evolution and they are potentially affected by noise. The density distribution was generated by considering the grey scale associated to the images: a significant amount of mass is produced (more than 50% of mass increase between the first and the last image of the sequence) and the geometrical configuration is non-trivial, in particular there is the creation of novel branches. We performed several numerical experiments and tested all the source model proposed. Hereafter, only the tests performed with the non-linear normal growth model are described, that gave the best performances in terms of interpolation.

The numerical experiments performed are the following. The mappings between the first image and the last three ones were computed and the interpolated images generated was compared to the original images. In Fig.15 the mass curve for three different mappings is considered. The red line represents the mass curve when the interpolation between images $(1-3)$ is constructed. The blue and the black line are the mass curve for the mappings $(1-4)$ and $(1-5)$ respectively. From a quantitative standpoint only the mapping $(1-3)$ provides a good, realistic result. As said, the error is mainly due to the 2D nature of the images.

The interpolation between the images $(1-5)$ is analyzed. The interpolated images (obtained by transport with the optimal mapping) are compared to the images of the sequence at corresponding time.

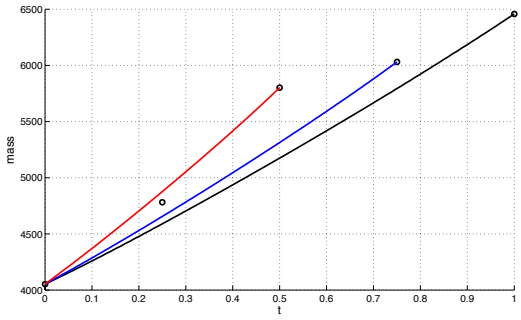

FIG 15. *Plot of the mass variation for the different interpolations. Red line is the mass curve when the interpolation between the first and the third images is considered, the blue and the black line are the mass curve for the interpolations between the first and the fourth and fifth images respectively.*

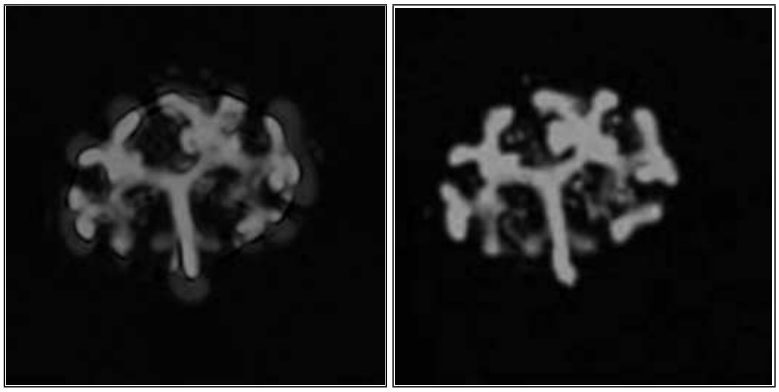

a) $\rho(0.25)$ b) $\overline{\rho}(0.25)$

FIG 16. *Comparison between the interpolation at time* $t = 0.25$*, a), obtained by solving optimal transport between images* $(1-5)$ *and the original image in grey scale b)*

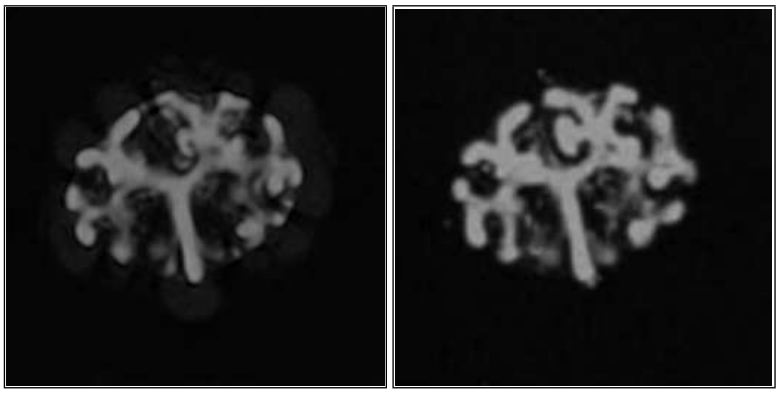

a) $\rho(0.50)$ b) $\overline{\rho}(0.50)$

FIG 17. *Comparison between the interpolation at time* $t = 0.5$*, a), obtained by solving optimal transport between images* $(1-5)$ *and the original image in grey scale b)*

The qualitative agreement between the interpolated images and the original one is quite good (see Fig.(16,17,18)). All the main geometrical features of the kidney tree are well reconstructed, even if only the first and the last image of the sequence are used to build the mapping.

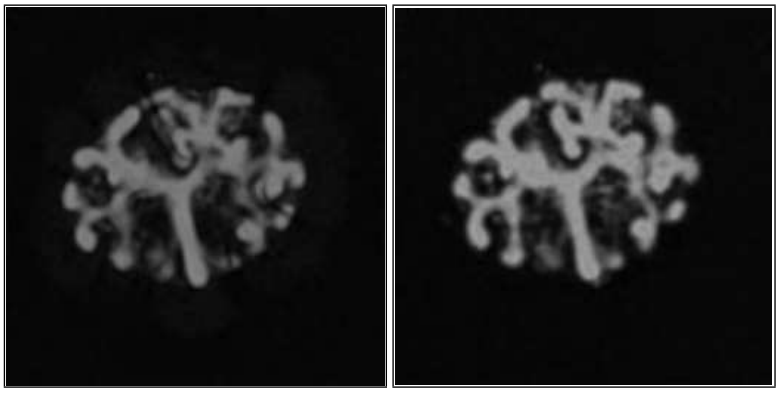

a) $\rho(0.75)$ b) $\overline{\rho}(0.75)$

FIG 18. *Comparison between the interpolation at time $t = 0.75$, a), obtained by solving optimal transport between images $(1-5)$ and the original image in grey scale b)*

7.3. Perspective: mass sources to model obstacles

A mass source of expression $S = -\rho D_t \Gamma$, with $\Gamma = \Gamma(x,t)$ may act as an obstacle. If the obstacle is fixed in space, then $\Gamma = \Gamma(x),\ S = -m \cdot \nabla\Gamma$.

This may be deduced by performing a change of variable in the action. In particular, let us consider the lagrangian:

$$\mathcal{L} = \int_0^1 \int_\Omega \frac{|m|^2}{2\rho} + \phi \left(\partial_t \rho + \nabla \cdot m + \rho \frac{D\Gamma}{Dt} \right) \, d\Omega \, dt. \tag{89}$$

A density variable σ defined as:

$$\rho := \sigma \exp(-\Gamma), \tag{90}$$

is introduced, that inserted into the lagrangian transform the problem into:

$$\mathcal{L} = \int_0^1 \int_\Omega \frac{1}{2} \sigma \exp(-\Gamma) |\mathbf{v}|^2 + \lambda \left(\partial_t \sigma + \nabla \cdot (\sigma \mathbf{v}) \right) \, d\Omega \, dt, \tag{91}$$

where λ is the Lagrange multiplier associated to the constraint on σ.

Let us remark that in this case the constraint is the usual one and the kinetic energy is modified by an isotropic metric term involving the exponential of the scalar field. The Euler-Lagrange equation for this system reads:

$$\partial_t \lambda + \mathbf{v} \cdot \nabla \lambda = \frac{1}{2} \exp(-\Gamma) \mathbf{v}^2, \tag{92}$$

$$\mathbf{v} = \exp(\Gamma) \nabla \lambda, \tag{93}$$

that, after substitution reduces to:

$$\partial_t \lambda + \frac{1}{2} \exp(\Gamma) |\nabla \lambda|^2 = 0. \tag{94}$$

In conclusion, every source term of the form $\rho D_t \Gamma$ acts in a dual manner. It may be considered as a source term or a metric factor.

8. Conclusion

In this paper we proposed a model of optimal transport between two unbalanced densities, which coincides with the usual transport in the balanced case. The model relies on the addition of a source term in the mass conservation equation. Three kinds of source terms are proposed and studied for application to tumor growth. For two of them, we propose an existence result for the optimal transport problem, and give numerical evidence of its convergence and ability to deal with mass growth in various tests cases where the usual transport fails. The key properties of our model are: a finite speed of motion of mass, and a the recovering of usual optimal transport for balanced densities, which was not the case of existing models for unbalanced densities [3, 15, 16].

Acknowledgment: We would like to thank Q. Mérigot who pointed out to us the references [15, 16]. E. Maitre is supported by French Agence Nationale de la Recherche, ANR Project TOMMI (ANR 2011 BS01 014 01) and by Grenoble INP, through SEI grant TOSCANA.

References

[1] L. Ambrosio and N. Gigli, *A user's guide to optimal transport*, in Modelling and Optimisation of Flows on Networks. Springer Berlin Heidelberg, pp. 1–155. (2013)

[2] S. Agenent, S. Haker and A. Tannenbaum, *Minimizing flows for the Monge-Kantorovich problem*, SIAM J. Math. Analysis, 35:61–97 (2003)

[3] J.-D. Benamou, *Numerical resolution of an "unbalanced" mass transfer problem*, ESAIM: Mathematical Modelling and Numerical Analysis Vol. 37, No 5, 851–868 (2003)

[4] J.-D. Benamou and Y. Brenier, *A computational fluid mechanics solution of the Monge-Katorovich mass transfer problem*, Numer. Math. 84:375–393 (2000)

[5] J.-D. Benamou and Y. Brenier, *Mixed L^2-Wasserstein optimal mapping between prescribed density functions*, J. Opt. Theory and Applications, 111, (2):255–271 (2001)

[6] J.-D. Benamou, Y. Brenier and K. Guittet *Numerical Analysis of a Multi-Phasic Mass Transport Problem*, Int. J. Numer. Meth. Fluids 40:21–30 (2002)

[7] JD Benamou, B Froese, A Oberman, *Numerical solution of the second boundary value problem for the Elliptic Monge-Ampère equation*, HAL preprint on hal.inria.fr (2012)

[8] J.-D. Benamou, B. Froese, A. Oberman, *Numerical Solution of the Optimal Transportation Problem via viscosity solutions for the Monge-Ampère equation*, arXiv preprint arXiv:1208.4873 (2012)

[9] R. McCann, *Polar factorization of maps on Riemannian manifolds*, Geom. Funct. Analysis, 11:589–608 (2001)

[10] E.J. Dean and R. Glowinski, *Numerical methods for fully nonlinear elliptic equations of the Monge-Ampère type*, Computer methods in applied mechanics and engineering, 195 (13-16):1344–1386 (2006)

[11] A. Figalli and N. Gigli, *A new transportation distance between non-negative measures, with applications to gradients flows with Dirichlet boundary conditions*, J. Math. Pures Appl. (9), 94 (2010), pp. 107ï£¡130.

[12] M. Fortin and R. Glowinski, *Augmented Lagrangian Methods: Applications to the Solution of Boundary Value Problems*, Studies in Mathematics and its Applications 15, North-Holland, Amsterdam (1983)

[13] G. Loeper and F. Rapetti, *Numerical solution of the Monge-Ampre equation by a Newton's algorithm*, C. R. Math. Acad. Sci. Paris, 340:319–324 (2005)

[14] R. Peyre, *Non-asymptotic equivalence between W_2 distance and H^{-1} norm*, Arxiv 2011

[15] B. Piccoli and F. Rossi, *Generalized Wasserstein distance and its application to transport equations with source*, Arxiv 2012

[16] B. Piccoli and F. Rossi, *A generalized Benamou-Brenier formula for mass-varying densities*, Arxiv 2013

[17] C. Villani, *Topics in optimal transportation*, Graduate Studies in Mathematics, Vol. 50, AMS (2003)